AGU PUBLICATIONS

JGR

Journal of Geophysical Research: Atmospheres

RESEARCH ARTICLE
10.1002/2014JD022699

Intercalibration of microwave temperature sounders using radio occultation measurements

O. Isoz[1], S. A. Buehler[2], and P. Eriksson[3]

[1]Department of Computer Science, Electrical Engineering and Space Technology, Luleå University of Technology, Luleå, Sweden, [2]Meteorological Institute, University of Hamburg, Hamburg, Germany, [3]Department of Earth and Space Sciences, Chalmers University of Technology, Gothenburg, Sweden

Key Points:
- Intercompare microwave temperature sensors using radio occultation
- Shows brightness temperature-dependent difference between AMSU-A sensors
- Shows the impact of the applied antenna corrections

Supporting Information:
- Figures S1–S4
- Figure S1
- Figure S2
- Figure S3
- Figure S4

Correspondence to:
S. A. Buehler,
stefan.buehler@uni-hamburg.de

Citation:
Isoz, O., S. A. Buehler, and P. Eriksson (2015), Intercalibration of microwave temperature sounders using radio occultation measurements, *J. Geophys. Res. Atmos.*, *120*, 3758–3773, doi:10.1002/2014JD022699.

Received 9 OCT 2014
Accepted 20 MAR 2015
Accepted article online 26 2015
Published online 8 May 2015

Abstract This is a study of the usefulness of radio occultation (RO) data for intercomparing different microwave temperature (MWT) sounding instruments. The RO data used are from the Global Navigational Satellite System Receiver for Atmospheric Sounding on the Metop-A and B satellites. The MWT sounders investigated are the Advanced Microwave Sounding Unit-A instruments on the satellites NOAA 15, 16, and 18 and Metop-A. We collocate RO and MWT data and then use these collocations to study various aspects of the MWT instruments. In addition, two different versions of the MWT data are compared: standard operational data (OPR) and the NOAA Integrated Microwave Intercalibration Approach data (IMICA). The time series of monthly mean differences shows that there are robust patterns for each satellite and data version, which mostly drift only slowly over time. The intersatellite spread, measured by the standard deviation of the yearly mean values by all satellites, is between 0.1 and 0.4 K, depending on channel, with no significant differences between OPR and IMICA data. The only notable exception is Channel 8 of NOAA 16, which appears to have a time-varying offset of 0.5–1 K relative to the other instruments. At this point it is not clear whether this deviation is real or a sampling artifact, so further study is needed. Due to the large number of collocations used, it is possible to also investigate the scene brightness and scan angle dependence of the MWT bias (relative to RO). First results of such an analysis are presented and discussed. Particularly, the investigation of the scan angle dependence is novel, since this bias pattern is difficult to assess without RO data. Further work is needed on these angular dependences, before conclusions are robust enough to include in data recalibration efforts, but our overall conclusion is that RO collocations are a powerful tool for intercomparing MWT sounders.

1. Introduction

There are different techniques to measure the temperature in the atmosphere as a function of altitude above ground. Some methods, such as radiosondes, measure the temperature in situ, while other sensors apply remote sensing. Radio occultation (RO) is an active technique that uses the signal from the Global Navigational Satellite System (GNSS) satellites to estimate the bending of the signal path caused by the atmosphere. The bending profile can be converted to a temperature profile with a high vertical resolution [*Jin et al.*, 2014]. RO instruments referred to in this article are the GNSS Receiver for Atmospheric Sounding (GRAS) and the RO instrument on the Constellation Observing System for Meteorology, Ionosphere, and Climate (COSMIC) satellites.

A more traditional alternative to RO measurements are passive observations at various wavelengths. In this article, we focus on the microwave spectral range and in particular the Advanced Microwave Sounding Unit-A (AMSU-A) family of instruments. They measure the emission from mainly oxygen in various frequency bands corresponding to different atmospheric pressure levels.

Each of these methods has its strengths and weaknesses. RO uses continuously monitored transmitters, and the receiver can be continuously calibrated using signals from other GPS satellites that do not propagate through the atmosphere [*Jin et al.*, 2014, section 6.2.4]. This significantly reduces instrument-specific biases, and RO receivers are often considered to be "self-calibrated." But since RO only can perform a measurement when the signal path between a GPS satellite and the receiver passes through the atmosphere, the number of soundings is limited to approximately 600 per day and receiver [*Jin et al.*, 2014, Table 5.2]. AMSU-A, on the other hand, measures thermal emission from the atmosphere, making it possible to measure the atmospheric temperature continuously independent of other instruments.

It is well known that measurements from passive instruments can be impacted by a number of factors. These include bias from radiation reflected off the spacecraft (causing a scan-related bias) [*Buehler et al.*, 2005], drift in the receiver oscillator [*Lu and Bell*, 2013], and other biases such as differences between the antennas on the different satellites and instrument-specific nonlinearities [*Zou et al.*, 2006; *Zou and Wang*, 2011]. The independence from other instruments means that the quality of the measurements will be highly dependent on the instrument itself and its unique characteristics [e.g., *Zou and Wang*, 2011; *Qin et al.*, 2012; *Doherty et al.*, 2012; *Lu and Bell*, 2013]. Therefore, a number of authors have suggested methods to intercompare and correct data from different AMSU-A sensors [e.g., *Mo*, 2011; *Zou and Wang*, 2011; *Doherty et al.*, 2012].

A particularly promising method is to use the aforementioned RO as a reference. One reason for this is the high consistency between different RO sensors [*Foelsche et al.*, 2011a]. Hence, a number of papers comparing RO with different passive sensors have been published. For example, *Schrøder et al.* [2003] applied the vertical weighting function for MSU Channel 4 to RO data and used the simulated brightness temperatures to create zonal means; these were then used to estimate the accuracy of MSU Channel 4 brightness temperatures. *Ho et al.* [2009] used "dry" RO profiles from the COSMIC satellites [*Anthes et al.*, 2008] to create simulated brightness temperatures for AMSU-A Channels 8–10; these were then compared with collocated AMSU-A measurements from NOAA 15, 16, and 18. Dry RO profiles contains no information about the water content of the air; therefore, they will underestimate the temperature at low altitudes.

He et al. [2014] compared NOAA operational and NOAA Integrated Microwave Intercalibration Approach (IMICA) AMSU-A observations with simulated AMSU-A Channel 9 brightness temperatures based on RO data from the COSMIC satellites. *Ho et al.* [2009] and *He et al.* [2014] only used scan angles within 15° of nadir and treated all soundings to be at nadir. *Steiner et al.* [2007, 2009] compared RO monthly climatologies with MSU/AMSU-A data. *Ladstädter* [2011] compared the AMSU-A instrument on board Metop-A to European Centre for Medium-Range Weather Forecasts (ECMWF) model data and to both wet and dry GRAS RO profiles, and *Ladstädter et al.* [2011] compared global temperature records based on AMSU-A, RO, and radiosondes. *Chen and Zou* [2014] did an extensive comparison between COSMIC-RO and AMSU-A Channels 5–11 on board NOAA 18 and estimated a new set of AMSU-A calibration factors. Last but not least, *Zou et al.* [2014] compared RO and the successor to AMSU-A, the Advanced Technology Microwave Sounder (ATMS). They compared ATMS data, collected during clear-sky conditions between 60°N and 60°S, with collocated GPS RO measurements.

This study employs the same basic methodology as most earlier comparisons: RO temperature profiles are used to simulate AMSU-A observations with a radiative transfer software. However, in contrast to most earlier comparisons, a full simulation is performed for each collocation and the complete scan range of AMSU-A is considered. This allows us to consider not only the basic difference between AMSU-A sensors but also how brightness temperature biases vary as a function of scan position and scene brightness, for each individual instrument. Hence, the ambition is to show that comparison with RO data allows to disentangle the contribution of different sources of brightness temperature biases. Another novel aspect is that this paper uses the GRAS instrument on Metop as the source of RO data instead of the RO receivers on board the COSMIC satellite series. GRAS has been reported to have a lower bending angle noise than COSMIC [*Foelsche et al.*, 2011a] and has been shown to have a lower standard deviation for measurements above 38 km altitude [*von Engeln et al.*, 2011].

Only AMSU-A Channels 8–13 are considered, since these channels are mainly sensitive to the altitude range where RO has the highest retrieval accuracy for temperature. Unfortunately, it is not possible to derive biases in an exact absolute sense. This as the methodology involves radiative transfer simulations, and there exist significant uncertainties around the spectroscopy of oxygen in the frequency range of concern. This results in systematic errors in simulated brightness temperatures, implying that primarily relative biases can be derived. The application on AMSU-A is only an example, the approach presented can equally well be applied on channels of other satellite temperature sounders targeting the lower stratosphere.

The paper starts by describing the two instrument series used in this study and how the collocations were done. Then the selected RO data are used to create simulated AMSU-A measurements, and these are compared to collocated actual AMSU-A measurements from several viewpoints, such as monthly mean differences and variations with scan angle and brightness temperature. Furthermore, the impact of two different antenna correction schemes on the AMSU-A measurements is shown. At the end of the paper, our results are compared to other studies before conclusions are drawn.

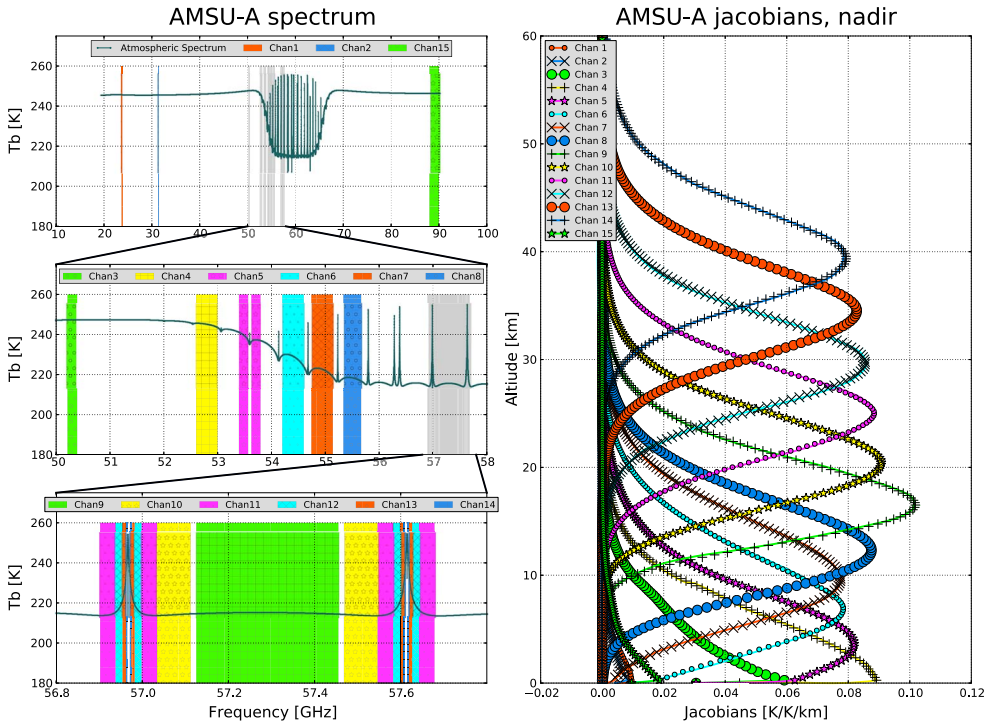

Figure 1. An overview over the channels of the AMSU-A sensor. (left) The position of the frequency passbands of each channel, on top of a simulated (monochromatic) spectrum. (right) The temperature Jacobians. The simulations are for nadir viewing angle and a subarctic winter atmospheric scenario.

2. Data and Method

By comparing the time and location for all available GRAS RO profiles with all AMSU-A data of the time period, a set of collocated measurements between the different instruments was extracted. After the extraction of the collocations, an atmospheric radiative simulator was used to simulate AMSU-A brightness temperatures based on the GRAS RO profiles. Bias estimates were obtained by comparing simulated AMSU-A brightness temperatures with collocated operational and recalibrated AMSU-A measurements.

2.1. The AMSU-A Instrument

Advanced Microwave Sounding Unit-A (AMSU-A) is a 15-channel microwave radiometer that has been used on both NOAA and European Organisation for the Exploitation of Meteorological Satellites polar orbiting satellites since 1998. The instrument measures emission from the Earth and the atmosphere at frequencies between 23.8 and 89 GHz, in a cross-track scan pattern with 30 steps covering a total swath width of about 2200 km. Figure 1 shows the frequency position and the altitude sensitivity of the channels. As can be seen in the figure, Channels 1–7 and 15 are to various degrees sensitive to emissions from the ground and are therefore unsuitable to be intercompared using the method in this paper. Channel 14 is located above the part of the atmosphere where the pressure is high enough to cause a significant bending of the signal used for RO. Therefore, this work is only analyzing the relative biases for Channels 8 to 13. These channels estimate atmospheric temperatures by measuring the emission at different pressure levels in the 57 GHz O_2 band. The standard operational calibration for AMSU-A is described in *Robel et al.* [2009].

2.2. AMSU-A Data Versions

Two different AMSU-A products are used in this paper: the NOAA operational L1c data (referred to as OPR) and the NOAA Integrated Microwave Intercalibration Approach data (IMICA), described in *Zou and Wang* [2013]. The IMICA data constitute the NOAA fundamental climate data record for AMSU-A and use an algorithm where the AMSU-A data are intercalibrated using simultaneous nadir overpasses (SNO) [*Zou et al.*, 2006; *Zou and Wang*, 2011] in order to reduce the intersatellite errors between different AMSU-A instruments.

2.3. RO-GRAS

Currently, there are a number of different RO receivers in orbit. Examples include the Chinese GNSS Occultation Sounder (used on board the F3C mission); the Integrated GPS Occultation Receiver family of receivers by Broad Reach/JPL, U.S. (used on board, e.g., the U.S./Taiwanese COSMIC series of satellites); and the GNSS Receiver for Atmospheric Sounding (GRAS) by RUAG Space, Sweden (used on board the European Metop series). *Foelsche et al.* [2011a] showed that there is almost no difference in accuracy between the different receivers/mission, although the noise of the GRAS measurements is significantly lower than the noise of the other RO receivers. Each receiver records approximately 600 occultations (measurements) each day [*Jin et al.*, 2014, Table 5.2]. The receiver uses the known position of the occulting GPS satellite and its own position to determine the impact of the atmosphere on the propagation of the GPS signal [*Jin et al.*, 2014, chap. 5 and 6]. Although RO measures temperature by limb sounding, *Foelsche et al.* [2011b] showed that it can provide a good reference for nadir sounding instruments. However, due to the movement of the satellites during an occultation, *Foelsche et al.* [2011b] showed also that an altitude-dependent error (compared to the temperature at the mean tangent point) may occur for measurements occurring at large distances from the flight path of the RO receiver. They state that the mean of the error is less than 0.5 K even at low altitudes. For occultations occurring closer to the RO receiver flight path, the estimated bias is smaller.

This paper uses data from the Global Navigational Satellite System (GNSS) Receiver for Atmospheric Sounding (GRAS) receiver model used on board the Metop series of polar-orbiting weather satellites. There are currently two Metop satellites in orbit, Metop-A was launched in October 2006 and Metop-B was launched in September 2012. The GRAS receiver on board Metop-B became operational in October 2012.

2.4. RO Data

The profiles used here are "wet" GRAS retrievals. This means that the profiles incorporate input from other sources to compensate for the impact from water vapor, in order to better estimate the temperature at low altitudes. In this case, the background data came from ECMWF analysis, and even if they are wet, the version of the GRAS Radio Occultation Meteorology Satellite Application Facility (ROMSAF) software applied to generate the profiles used here is not restricted as much by background data as later versions of the ROMSAF processing software (J. K. Nielsen, ROMSAF, The Danish Meteorological Institute (DMI), personal communication, 2014).

The RO method is most accurate between 8 and 30 km altitude, where the atmosphere is dense enough to cause a significant bending and dry enough for the water vapor impact to be negligible. RO data used in this study had the temperature calculated at 91 different pressure levels. *Kursinski et al.* [1997] estimated the vertical resolution to be approximately 1 km, but this depends somewhat on the exact retrieval algorithm used.

For Metop-A, the RO profiles are from January to August 2012 and October to December 2012, and for Metop-B, the RO profiles are only from October to December 2012. Unfortunately, ROMSAF was unable to deliver any RO data for September 2012.

The ROMSAF RO files contain an error estimate, "Temp_sigma." This variable gives the estimated σ for each temperature and altitude. The mean Temp_sigma between 8 and 25 km altitude is below 0.5 K. It is below 1.5 K up to an altitude of approximately 37 km.

2.5. Comparison Method

Our collocation criteria are that the GRAS and AMSU-A measurements should occur within 1 h in time and 150 km in distance. The location used for AMSU-A measurements is the center of the AMSU-A sensor ground footprint, and the location for RO is where the straight line between the GPS satellite and the receiver touches the surface of the Earth during the occultation. If multiple AMSU-A soundings fulfilled the criteria with respect to one RO measurement, the closest one in distance was selected. The mean distance between the RO and AMSU-A soundings, in the set of collocations obtained, is 30 km in distance on the ground and 25 min in time.

In principle, the more correct approach to the collocation problem would be to assign different positions (latitude/longitude) to an RO measurement, depending on what AMSU channel it is being compared to. One would then chose as RO position the latitude/longitude where the occultation "beam" is at the altitude of maximum sensitivity of the selected AMSU channel. But *Feltz et al.* [2014] showed that for IR-based sounders in the polar regions our much simpler approach only increases the root-mean-square error for temperatures

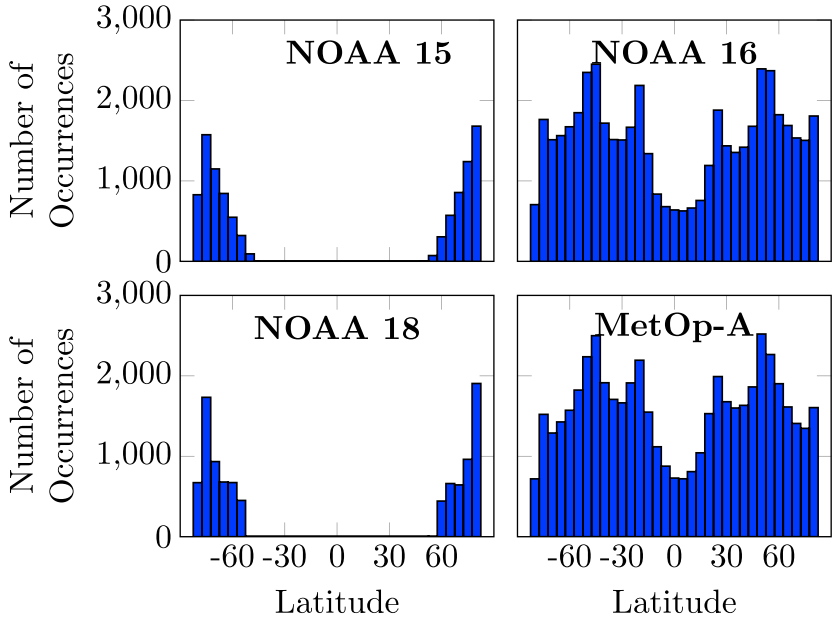

Figure 2. Distribution in latitude of the collocations found for each AMSU-A sensor considered.

at the 100 hPa level (approximately 17 km altitude) by 5–10%, compared to the more correct treatment. We therefore judge our simple treatment of using only one position for the entire RO measurement to be adequate for the purpose of this study.

The exact latitude distribution of the collocations varies between the AMSU-A sensors, but most collocations are found at high latitudes. Figure 2 shows a histogram of all collocations. As can be seen, only two of the four satellites obtain global collocations; the reason for this is the different orbits used by the satellites. Due to the distribution of the collocations, this study uses only collocations occurring in the area poleward of 60°N and 60°S.

The retrieved RO temperature profiles were used to generate simulated AMSU-A radiances using the open source Atmospheric Radiative Transfer Simulator (ARTS) [*Eriksson et al.*, 2011]. For this work, a full 3-D simulation was done for each collocated AMSU-A measurement, using the location of the AMSU-A sensor platform together with the scan angles of the AMSU-A antenna. The vertical profiles of temperature and specific humidity of the atmosphere were taken from the RO data, and it was assumed that the atmosphere was horizontally homogeneous. To speed up the calculations, absorption cross sections were precalculated and stored in lookup tables, as described in *Buehler et al.* [2011]. The spatial resolution was treated to be infinite (pencil beam), while the frequency response was carefully incorporated by using a dense monochromatic frequency grid and assuming rectangular channel responses with widths taken from *Robel et al.* [2009]. The sensor was applied to the simulated monochromatic radiances by a straightforward matrix multiplication, as described in *Eriksson et al.* [2006]. Absorption due to oxygen was calculated following *Rosenkranz* [1993]. ARTS is well validated for the simulation of downward looking microwave sensors, in general [e.g., *Buehler et al.*, 2006], but it has so far not been used for the AMSU-A channels in particular.

The simulations contain some systematic uncertainties, for example, due to assumptions on spectroscopic parameters [cf. *Verdes et al.*, 2005]. We estimate the absolute accuracy of the simulations to be approximately 1 K. This value is mostly based on the experience from various intercomparison campaigns [e.g., *Melsheimer et al.*, 2005], reflecting the initial intermodel spread, before spectroscopic parameters and interpolation strategies were tuned to match exactly. But since these inaccuracies can be assumed to impact all satellites equally and we do not try to do any absolute calibration of the AMSU-A instruments, it is not likely that the limited accuracy will impact our results.

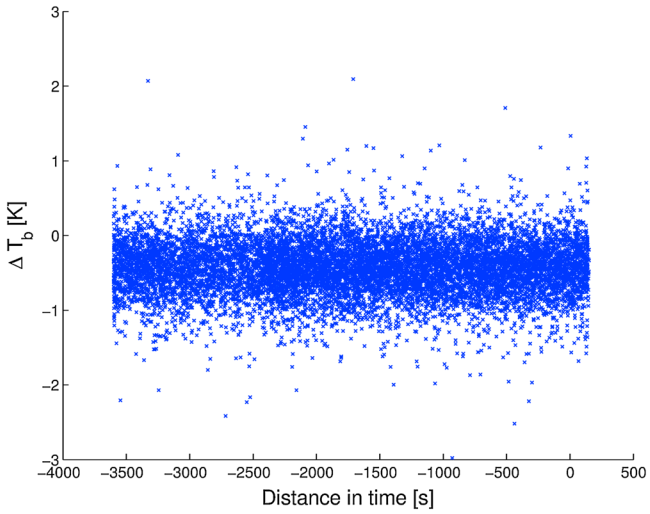

Figure 3. Brightness temperature difference (observation-reference, equation (2)) as a function of time difference between AMSU-A and RO observations. The AMSU-A data are for NOAA 15, Channel 8, and the OPR data version.

3. Results and Discussion

3.1. Validation of the Collocation Criteria

After the collocations between RO and AMSU-A were identified, an initial validation was done before further analysis. An AMSU-A sounding has a diameter of approximately 50 km in nadir and increases toward the edges of the AMSU-A swath. This means that if the collocated AMSU-A sounding is at nadir and the distance is below 22.5 km, the RO reference position is inside the AMSU-A sounding. For collocations occurring farther away from nadir, the maximum distance where the RO reference point will still be inside the AMSU-A ground footprint increases. To determine how the difference between AMSU-A and RO changed when the distance in time or space was increased, a visual inspection was done for all channels and all satellites versus the difference in time or space. As an example, the two plots for AMSU-A Channel 8 on NOAA 15 are displayed in Figures 3 and 4.

Figure 3 shows the difference between RO and AMSU-A versus time difference between the soundings. Essentially no time dependence can be seen; this indicates that it should be possible to relax the time criteria for the collocations in a future study. The next figure, Figure 4, shows the difference between RO and AMSU-A

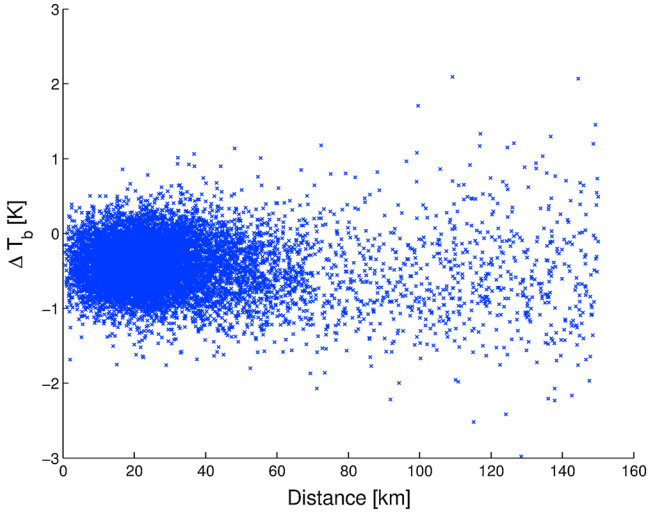

Figure 4. Brightness temperature difference (observation-reference, equation (2)) as a function of spatial distance between AMSU-A and RO observations. The distance is calculated at ground level. The AMSU-A data are for NOAA 15, Channel 8, and the OPR data version.

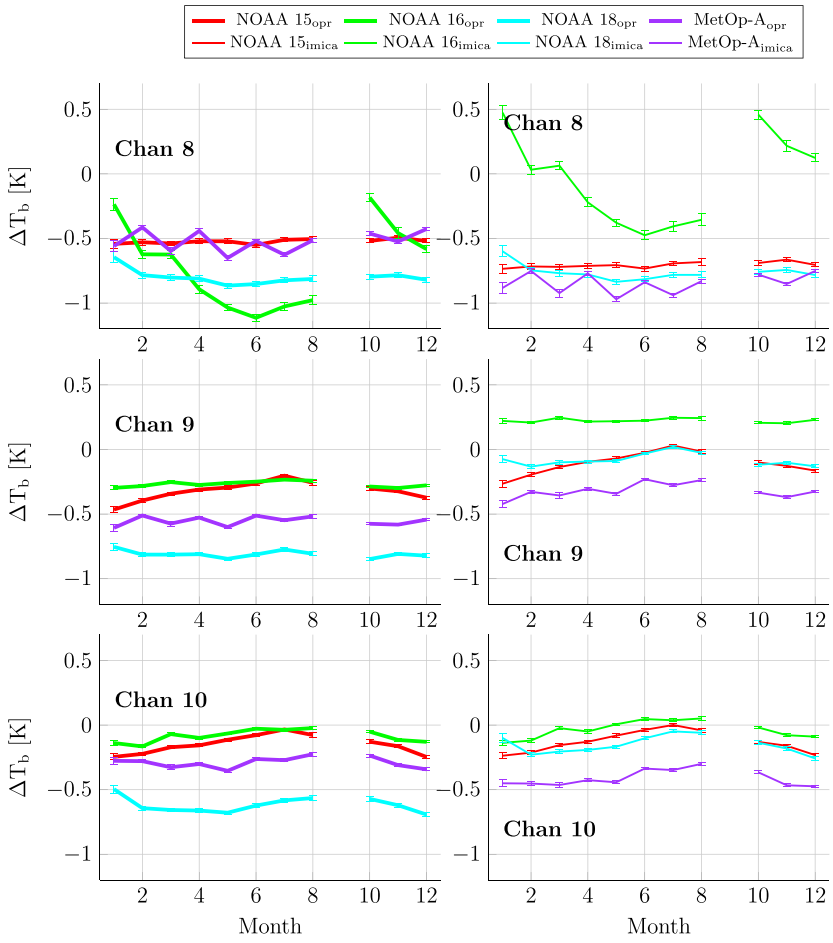

Figure 5. Monthly mean brightness temperature difference (observation-reference, equation (2)) for (top to bottom rows) Channels 8–10 and different data version with (left/right column) OPR/IMICA. Only AMSU-A data from the eight footprints closest to nadir and poleward of 60° latitude were used. No RO data were at hand for September. The uncertainty (±1 SE, equation (1)) for each data point is indicated as a vertical bar.

versus spatial collocation distance. Based on Figure 4 in *Zou et al.* [2006], we expect the brightness temperature difference to increase with spatial distance, especially above distances of approximately 100 km. There are indeed a few data points for which this is the case, but they are too rare to affect the calculated averages. Most of our collocation pairs are at differences below approximately 60 km. Overall, we conclude that our spatial and temporal collocation criteria are appropriate.

3.2. Overall Level of Agreement

In order to reduce any scan-related issues, statistics were here derived only on data from the eight sensor positions closest to nadir. In addition, to further homogenize the data set, only data poleward of 60°N/S were used. Monthly averages were calculated, and the number of collocations each month varied between 40 and 1900 for the different months and sensors. Most collocations occurred during October through December due to the inclusion of data from the GRAS receiver on board Metop-B.

Figures 5 and 6 show the monthly mean and the monthly standard error (SE) of the difference between RO/ARTS and AMSU-A for the different satellites and months. The standard error is calculated as

$$\mathrm{SE} = \sigma / \sqrt{N_{\mathrm{measurements}}}, \tag{1}$$

where σ is the standard deviation of the differences between the collocated AMSU-A and RO/ARTS soundings. In other words, we assume that the errors in the individual collocations are uncorrelated; then SE represents the standard deviation of the sample mean.

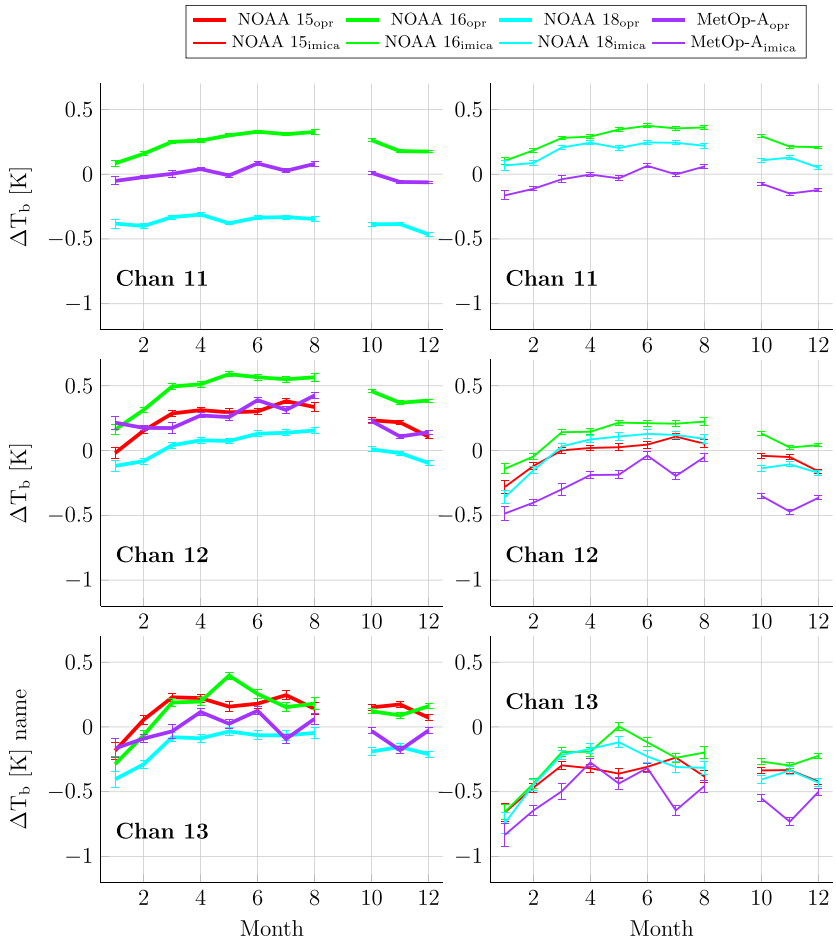

Figure 6. Same as Figure 5 but for Channels 11–13.

The assumption of no correlation is justified, given how the collocation set was constructed (only one matched AMSU-A measurement for each GRAS measurement and GRAS measurements being relatively sparse). The SE was found to be between 0.009 and 0.11 K and is shown in the plots throughout as error bars. The ΔT_b in the figure labels refers to

$$\Delta T_b = T_{b,\text{AMSU-A}} - T_{b,\text{RO/ARTS}}, \tag{2}$$

where $T_{b,\text{AMSU-A}}$ is the measured radiance from the AMSU-A sensor and $T_{b,\text{RO/ARTS}}$ is the simulated AMSU-A value based on RO.

For most channels, monthly mean ΔT_b varies smoothly with time. In addition, even if the number of collocations significantly increases in October, no significant change in the monthly mean brightness temperatures can be seen. This means that our method is not particularly sensitive to the number of collocations used in the comparison. Since the difference between the individual instruments and RO/ARTS is different for OPR and IMICA, it is clear that IMICA applies different corrections to the different AMSU-A instruments. In Channel 8, two instruments are significantly different to the others, NOAA 16 and Metop-A. NOAA 16 shows a significant change during the 12 month period; this change is clearly inconsistent with the other AMSU-A measurements and has a strong temporal variation, which is also not improved in the IMICA data relative to the OPR data; one reason could be a change in frequency of the onboard local oscillator causing a bias shift in the sensor [*NOAA*, 2012].

At this point we are not completely sure whether the unusual behavior of NOAA 16 Channel 8 is real or whether it represents some kind of sampling artifact. Global ocean mean and global land mean data do not show this behavior, according to a personal communication by one of the reviewers. Our comparison is restricted to

Table 1. Means of All Monthly Values and Associated Standard Deviations (in Parentheses) for the Difference Between AMSU-A and RO/ARTS for Both Investigated Data Sets[a]

Satellite	OPR Mean (σ)	IMICA Mean (σ)	Satellite	OPR Mean (σ)	IMICA Mean (σ)
	Channel 8			*Channel 11*	
NOAA 15	−0.52 (0.43)	−0.71 (0.44)	NOAA 15	- (-)	- (-)
NOAA 16	−0.70 (0.85)	−0.04 (0.98)	NOAA 16	0.24 (0.34)	0.27 (0.36)
NOAA 18	−0.80 (0.46)	−0.76 (0.47)	NOAA 18	−0.37 (0.34)	0.16 (0.37)
Metop-A	−0.52 (0.42)	−0.84 (0.43)	Metop-A	0.00 (0.36)	−0.05 (0.40)
Mean	−0.64 (0.14)	−0.59 (0.37)	Mean	−0.04 (0.31)	0.13 (0.16)
	Channel 9			*Channel 12*	
NOAA 15	−0.32 (0.31)	−0.11 (0.30)	NOAA 15	0.24 (0.51)	−0.04 (0.53)
NOAA 16	−0.27 (0.25)	0.22 (0.28)	NOAA 16	0.45 (0.53)	0.10 (0.54)
NOAA 18	−0.81 (0.29)	−0.08 (0.27)	NOAA 18	0.03 (0.48)	−0.03 (0.59)
Metop-A	−0.55 (0.30)	−0.32 (0.30)	Metop-A	0.25 (0.52)	−0.28 (0.64)
Mean	−0.49 (0.25)	−0.07 (0.22)	Mean	0.24 (0.17)	−0.06 (0.16)
	Channel 10			*Channel 13*	
NOAA 15	−0.15 (0.29)	−0.13 (0.30)	NOAA 15	0.13 (0.75)	−0.37 (0.76)
NOAA 16	−0.08 (0.28)	−0.03 (0.30)	NOAA 16	0.13 (0.78)	−0.26 (0.81)
NOAA 18	−0.62 (0.34)	−0.15 (0.32)	NOAA 18	−0.15 (0.69)	−0.34 (0.85)
Metop-A	−0.29 (0.33)	−0.41 (0.33)	Metop-A	−0.03 (0.77)	−0.54 (0.92)
Mean	−0.29 (0.24)	−0.18 (0.16)	Mean	0.02 (0.14)	−0.38 (0.12)

[a]Only AMSU-A data from the eight footprints closest to nadir and poleward of 60° latitude were used. Values are shown for each satellite. Rows labeled "Mean" show the mean of all the monthly satellite means and the associated standard deviation. Channel 11 on NOAA 15 failed in 2002 [*Wang and Zou*, 2014].

only high-latitude data (see Figure 2) which could be the explanation for the discrepancy. Another explanation could be a sampling artifact, since the exact collocation locations depend on the orbits of the involved satellites. However, we checked the collocation patterns carefully and could not find any obvious explanation there. This issue should be studied further.

The other slightly unusual satellite, Metop-A, shows a weak bimonthly pattern. This pattern occurs on both the Northern and Southern Hemispheres. At present we have no explanation for this pattern, but its amplitude is small, only approximately 0.1 K.

For the higher-altitude channels 11–13 (Figure 6), all AMSU-A instruments show a common pattern of deviation from GRAS. These channels also show significant seasonal variations between the Northern and Southern Hemispheres for all satellites. Due to the seasonal variations in the mean temperature of the collocated data, one possibility is that these variations are caused by the temperature-dependent biases discussed in section 3.3.

The annual mean differences between AMSU-A and RO/ARTS for all satellites are shown in Table 1. It is interesting to compare IMICA to OPR data. We base this discussion on the standard deviations of the mean values reported in the table. These are the standard deviations associated with calculating the mean over all satellites, so they represent the intersatellite spread. For Channel 8, this intersatellite spread actually gets slightly worse in IMICA (0.37 K instead of 0.14 K for OPR), largely because of the NOAA 16 issue with this channel, which is even more pronounced in IMICA than in OPR.

For Channels 9, 12, and 13, the intersatellite spread in IMICA is approximately the same as in OPR. For Channels 10 and 11 the intersatellite spread in IMICA is lower than in OPR. So overall, a mixed picture emerges. IMICA indeed reduces intersatellite spread for some channels but even increases it for one channel.

3.3. Scene Brightness Temperature Dependence

Another way to look at the data is to plot the difference between AMSU-A and RO/ARTS as a function of brightness temperatures; this is done in Figure 7. As in Figures 5 and 6, only the eight scan directions closest

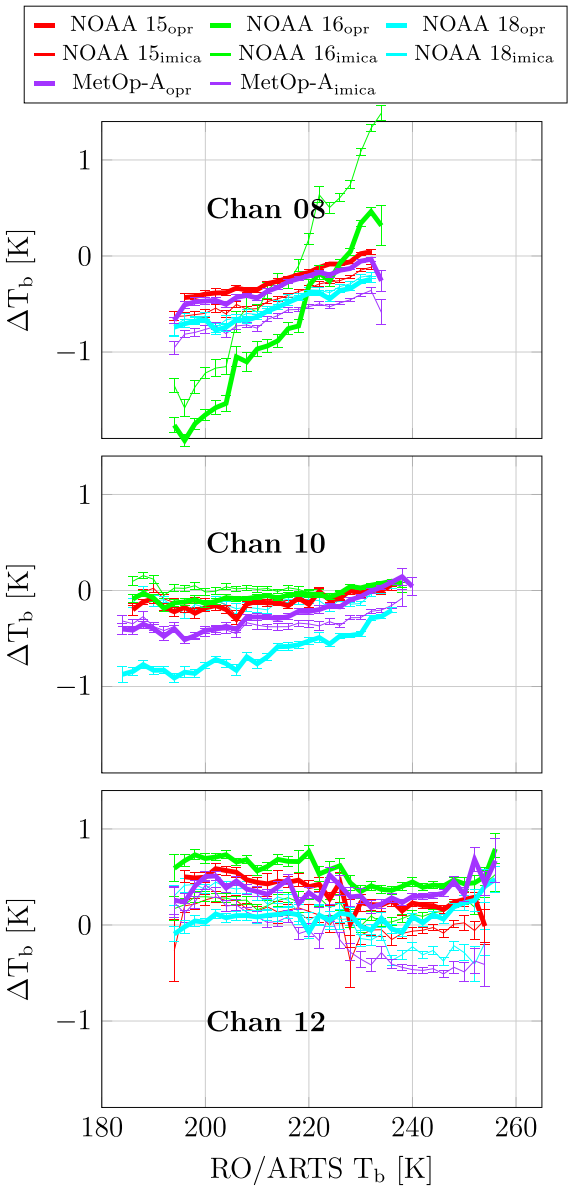

Figure 7. Difference between AMSU-A and GRAS for different RO/ARTS brightness temperatures for Channels 8, 10, and 12. The markers show the mean; vertical lines show the mean ±1 SE. This plot used near-nadir data. (See supporting information for other channels.)

to nadir and poleward of 60° latitude are used, and data from all available months are used. The mean and SE were calculated in bins of 2°K.

The figure shows that the difference between RO/ARTS and AMSU-A changes with the scene brightness temperature. For both Channels 8 and 10, there is a small increase in ΔT_b with increasing brightness temperature. For Channel 8, IMICA increases the difference for Metop-A and NOAA 15 fairly evenly for all brightness temperatures, NOAA 18 shows a small decrease, and NOAA 16 shows a significant change in difference due to the temperature. No obvious reason was found for this behavior. Channel 10 shows a much smaller temperature dependent difference, here IMICA significantly decreases the difference for NOAA 18. For the other satellites the change is smaller but so is the OPR temperature difference. Figure 7 (bottom), Channel 12, shows a slightly different pattern where the difference generally is becoming more negative for increased brightness temperatures, until it reaches temperatures around 250 K, where the difference starts to become more positive. For all sensors, IMICA has a negative bias correction at the higher brightness temperatures, but for lower brightness temperatures, NOAA 18 has a positive correction, whereas the other satellites have a negative correction also at those temperatures.

Other channels (9, 11, and 13) are not shown in the figure but are included in the supporting information to this article. Channel 9 behaves much like Channel 8, except that the NOAA 16 anomaly is largely missing (there is a slight hint of it for the IMICA data). Channel 11 has a quite flat bias behavior across the entire brightness temperature range. Channel 13 behaves much like Channel 12 but with a more pronounced negative slope for not too warm brightness temperatures (below approximately 250 K).

3.4. Scan Angle Dependence

Figure 8 shows that we have a sufficient number of collocations at all AMSU-A scan angles to investigate the scan angle dependence of the biases. The result of such an analysis is shown in Figure 9, which shows the difference between AMSU-A and RO/ARTS as a function of the AMSU-A scan angle. There is a significant asymmetric scan angle dependence in this difference for both the OPR and the IMICA data. For near-nadir data, the change in ΔT_b with angle is very small for all channels. But even for these data it might cause a slight negative bias on the results, compared to if only true nadir soundings were used in the comparison. The reason for the scan angle-dependent biases, in general, is that neither the standard NOAA OPR data nor the

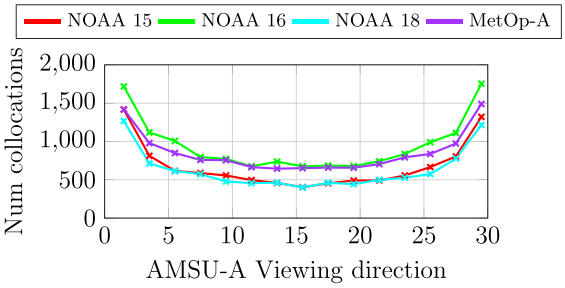

Figure 8. Number of collocations in the different AMSU-A viewing directions.

IMICA data contain any form of antenna correction.

3.5. Operational Antenna Corrections

Antenna corrections are currently used by the European Numerical Weather Prediction Satellite Application Facility (NWPSAF) and optionally by NOAA. NWPSAF uses the software package "AAPP" [*Labrot et al.*, 2014] where antenna corrections are applied by default. NOAA has the option to apply antenna corrections, but they do not use them by default. The two agencies apply different schemes, and the impact on the AMSU-A data is slightly different.

AAPP is based on the following equation [*Hewison and Saunders*, 1996, equation (10)]:

$$B_E = \frac{B_{\text{Ant}} - \eta_S B_S - \eta_P B_P}{\eta_E}, \tag{3}$$

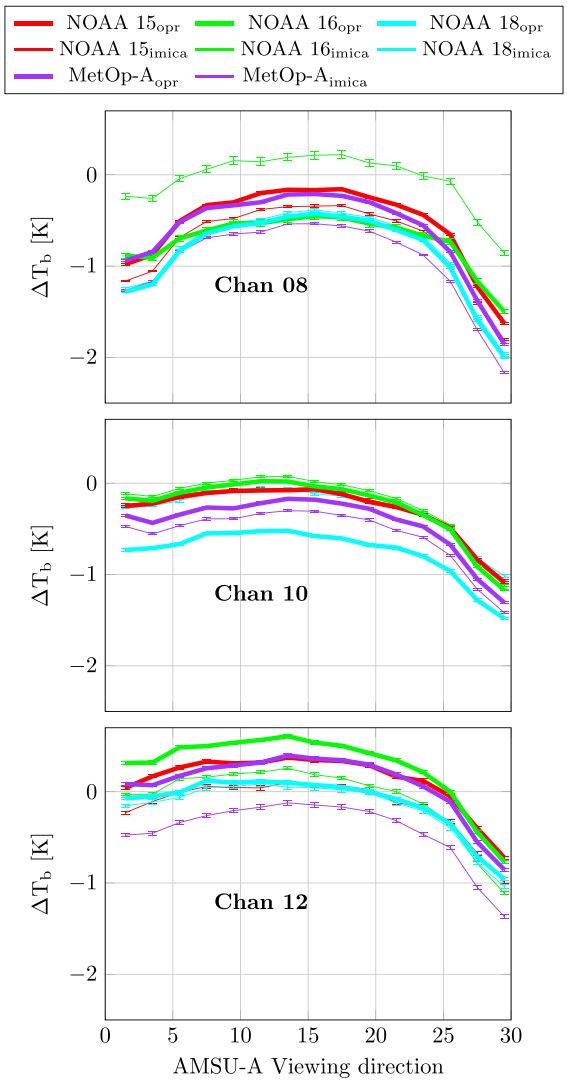

Figure 9. Difference between AMSU-A and GRAS for different AMSU-A viewing angles for Channels 8, 10, and 12. (See supporting information for other channels.)

where B_E, B_P, and B_S refer to the radiances from Earth, satellite platform, and space, respectively. The angular-dependent efficiencies are η_E, η_P, and η_S at which the antenna detects radiation from Earth, the satellite platform, and space. It is assumed that B_S is the Planck radiance for 2.73 K and that the platform mainly reflects emission from the Earth, causing the platform brightness temperature to be approximately the same as the Earth brightness temperature, so $B_P \approx B_E$. The different η parameters in AAPP are tabulated for different channels, satellites, and scan angles, but the actual values are so far set to be identical for all satellites, although NOAA 18 and Metop-A have an additional set of values that are not used by default.

NOAA uses a similar equation developed in *Mo* [1999],

$$T_E = \frac{T_{\text{Ant}}\left(\eta_E + \eta_C\eta_P + \eta_S\right) - 2.73\eta_s - \eta_C\eta_P T_P}{\eta_E}. \tag{4}$$

Here the calculations are done using brightness temperatures and not radiances. T_E is the brightness temperature of the Earth, and η_C is a channel-dependent correction for the antenna near field of the emission from the platform. The assumed brightness temperature of the space view is 2.73 K. For the NOAA algorithm, the combined antenna efficiency for each viewing angle, $\eta_E+\eta_S+\eta_P$, is explicitly normalized to 1. For AAPP it is not explicitly

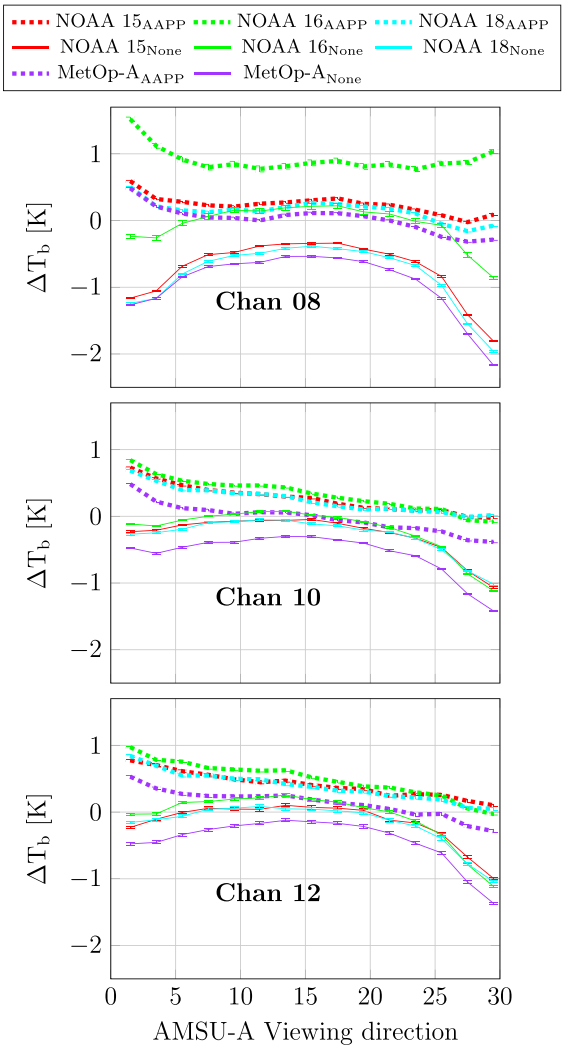

Figure 10. Difference between AMSU-A and GRAS for different AMSU-A viewing angles for Channels 8, 10, and 12. The data used for this plot are IMICA data. The dotted lines show the differences after the AAPP antenna correction scheme has been applied. (See supporting information for other channels.)

stated that the sum of the efficiencies is normalized, but it seems to be the case. The contribution to the bias from the satellite radiation can be considered to be negligible, since $\eta_C \eta_P T_P \approx 0.01$ K. Despite the slight difference in the expressions, the actual correction schemes are quite similar. However, the most significant difference is that in the NOAA scheme the parameters are different for each individual satellite.

Since the previous section showed that both the IMICA and OPR data sets had the same antenna dependence, we will only use the IMICA data set to show the impact of two antenna correction schemes. Figure 10 shows the scan-dependent difference for not antenna-corrected AMSU-A soundings compared to soundings corrected by the AAPP algorithm; that is, T_E is considered instead of T_{ANT}. Figure 11 shows the same for the NOAA antenna correction algorithm. By comparing Figures 10 and 11, it can be seen that NOAA uses different antenna patterns for each sensor, since the difference between IMICA and IMICA with the NOAA antenna correction applied varies for all satellites and viewing angels, whereas the difference between IMICA and IMICA with the AAPP antenna corrections is constant for all satellites. The scan-dependent difference decreases with both algorithms (Figures 10 and 11). For some channels and instruments, it seems to be possible to reduce the difference between the different instruments by adding the NOAA antenna correction after the IMICA algorithm has been applied to the AMSU-A data. The impact of the AAPP algorithm is mixed; the algorithm works fine for Channel 8 for all satellites except NOAA 16. But for Channels 10 and 12 the nadir difference increases for all but Metop-A. This is likely to be caused by the usage of the same antenna correction values for all instruments. The NOAA algorithm shows the same pattern, where the difference is reduced for two of the four sensors at Channel 8, but for Channels 10 and 12 the difference generally increases in nadir. The likely reason for this is that the IMICA algorithm does not use antenna corrections. Applying the correction afterward likely leads to overcorrection of those intersatellite differences that are, in fact, due to antenna differences.

3.6. Comparisons With Other Measurements

Our results are compared with some previous results in Table 2. The column "type" in the table indicates the combinations of RO data source and the type of AMSU-A data that have been analyzed. Unfortunately, in some cases it is not clear if the comparison is done using the data that are called OPR in this paper, although it can be assumed that the data used by *Zou and Wang* [2013] and *He et al.* [2014] are the same as the OPR data used in this paper. *Ho et al.* [2009] used operational AMSU-A data.

All previous studies in the table used data from the Taiwanese/American COSMIC satellites [*Anthes et al.*, 2008] receiver as the RO temperature reference. *Zou and Wang* [2013] and *He et al.* [2014] compared OPR- and IMICA-calibrated AMSU-A radiances for Channel 9 with COSMIC dry temperatures that had been converted

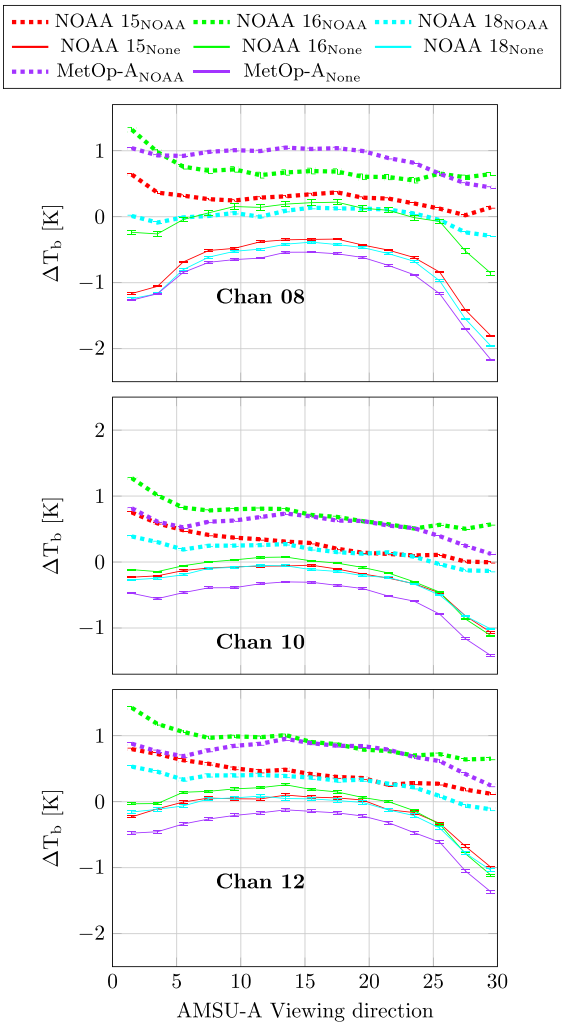

Figure 11. Same as Figure 10 but for the NOAA antenna correction scheme. (See supporting information for other channels.)

to simulated AMSU-A brightness temperatures using a forward radiative transfer model. That paper showed a significant improvement due to the implementation of the IMICA algorithm for the NOAA 15, NOAA 16, and NOAA 18 sensors. Compared with the results presented in *He et al.* [2014], if our results for Channel 9 are divided into the same longitudinal bands, then our comparison agrees with *He et al.* [2014] within 0.1 K for the northern polar region, but we have a much better agreement between RO and AMSU-A for all satellites in the southern polar region. The seasonal variations for Channel 9 show a smaller but similar pattern for the southern polar regions, but for the northern regions, our results have a clearer seasonal variation that seems to be less noisy.

Doherty et al. [2012] analyzed the difference between the successor to AMSU-A, ATMS, and AMSU-A on board NOAA 18, 19, and Metop-A using numerical weather prediction model fields as a reference. The results presented here have a significantly lower bias than what is shown in *Doherty et al.* [2012, Figure 10]. For example, for Channel 9, the difference between our measurements and the results by *Doherty et al.* [2012, Figure 10] is approximately 1 K. Figure 9 (middle and bottom) shows a similar shape of the directional bias as the corresponding panels in *Doherty et al.* [2012, Figure 3] but with a different offset. *Ho et al.* [2009] used the RO constellation COSMIC to estimate the bias in brightness temperatures between NOAA 15, 16, and 18. After dividing our data into the same latitudinal regions as they did, our results give approximately half the difference between RO and AMSU-A data on Channel 9 for all satellites and both polar regions, compared to *Ho et al.* [2009, Table 2]. For Channel 8, the results in that paper agree well with our results. Channel 10 shows a significant discrepancy; for NOAA 15 they estimate the global difference to be 1.5 K, whereas our results are 0.1 K. For the other satellites, the differences are smaller for that channel. There are a few possible reasons for the difference, one is the limited amount of data points (*Ho et al.* [2009] used between 150 and 350 collocations for each instrument on Channel 8 and 10 and between 500 and 800 for Channel 9) and another is changes in the instruments between the times of comparison.

Due to the number of variables involved in a collocation study, it is unlikely that different collocation studies would give exactly the same result. This is particularly clear when Table 4-1 in *He et al.* [2014] is compared to the results in *Zou and Wang* [2013]; these data were derived by the same research institute, yet the results differ.

4. Conclusions

We show that GRAS/RO profiles can be used to validate AMSU-A data. Similar studies have been done for other radio occultation instruments, and our results are overall reasonably consistent with the reported results. We also indirectly show that the addition of data from the GRAS receiver on board Metop-B does not generate any measurable change in the comparison result. The comparison produces stable results, and no significant

Table 2. Estimated Differences Between RO and AMSU-A for Different Articles[a]

Reference	Sattelite	Channel	Month	Type	N60–N90	S60–S90
Zou and Wang [2013]	NOAA 15	Ch 9	July 2007	OPR-COSMIC	−0.06	−0.82
He et al. [2014]	NOAA 15	Ch 9	July 2007	OPR-COSMIC	−0.22	−0.68
This paper	NOAA 15	Ch 9	July 2012	OPR-GRAS	−0.16	−0.26
Ho et al. [2009]	NOAA 15	Ch 9	September 2006	Oper-COSMIC	−0.47	−0.67
This paper	NOAA 15	Ch 9	August and October 2012	OPR-GRAS	−0.28	−0.29
Zou and Wang [2013]	NOAA 15	Ch 9	July 2007	SNO-COSMIC	0.07	−0.31
He et al. [2014]	NOAA 15	Ch 9	July 2007	SNO-COSMIC	−0.05	−0.38
This paper	NOAA 15	Ch 9	July 2012	SNO-GRAS	0.02	0.04
He et al. [2014]	NOAA 16	Ch 9	July 2007	OPR-COSMIC	−0.30	−0.67
This paper	NOAA 16	Ch 9	July 2012	OPR-GRAS	-0.14	−0.33
He et al. [2014]	NOAA 16	Ch 9	July 2007	SNO-COSMIC	−0.07	−0.32
This paper	NOAA 16	Ch 9	July 2012	SNO-GRAS	0.41	0.08
Ho et al. [2009]	NOAA 16	Ch 9	September 2006	OPR-COSMIC	−0.54	−1.2
This paper	NOAA 16	Ch 9	August and October 2012	OPR-GRAS	−0.29	−0.24
He et al. [2014]	NOAA 18	Ch 9	July 2007	OPR-COSMIC	−0.86	−1.42
This paper	NOAA 18	Ch 9	July 2012	OPR-GRAS	−0.60	−0.94
Ho et al. [2009]	NOAA 18	Ch 9	September 2006	OPR-COSMIC	−0.81	−1.92
This paper	NOAA 18	Ch 9	August and October 2012	OPR-GRAS	−0.79	−0.87
He et al. [2014]	NOAA 18	Ch 9	July 2007	SNO-COSMIC	−0.24	−0.50
This paper	NOAA 18	Ch 9	July 2012	SNO-GRAS	0.02	0.02

[a]OPR is operationally calibrated AMSU-A data; SNO stands for data calibrated using simultaneous nadir overpasses.

change in the observations occurs when the number of collocations doubles during the last quarter of the investigated year due to the addition of Metop-B.

Since we do the comparison between GRAS/RO and AMSU-A on a sounding by sounding basis, we can compare RO/ARTS with the OPR and IMICA data in novel ways, compared to earlier studies. In particular, the results are stable and detailed enough to investigate the scene brightness temperature dependence and the scan angle dependence of the bias. Both of these issues are very interesting. On the first issue, our results show that even the recalibrated and homogenized IMICA AMSU-A data still have scene brightness-dependent biases.

Concerning scan angle-dependent biases, we find clear indications of the presence of this issue, which is similar in OPR and IMICA data, i.e., which was not addressed by the homogenization. We also show that antenna corrections can be used to reduce the scan-dependent biases, but unfortunately, antenna corrections also affect nadir radiances and thus remove the benefit of homogenization if applied afterward. We conclude that it may be worthwhile to include in the future antenna aspects in the homogenization procedure.

Concerning the overall quality of the IMICA AMSU-A data, they seem to mostly fulfill the intersatellite accuracy of 0.2 K stated in *Zou and Wang* [2013]. The notable exception appears to be Channel 8 on NOAA 16, which in our analysis has a large discrepancy to the other satellites. This manifests itself in the time series (Figure 5) but even more clearly in the scene brightness dependence (Figure 7). It should be kept in mind here that our analysis is dominated by high latitudes (compare Figure 2), which may explain why the bias does not show up in other global comparisons that put more weight on the tropics and subtropics. Further work is necessary in order to confirm whether this represents a real bias in the microwave data or whether it is a sampling artifact due to the locations of the RO collocations for this particular satellite.

Acknowledgments
We thank ROMSAF for providing us with the GRAS temperature profiles and the ARTS community for providing the ARTS software. The GRAS RO data were provided by Kent Bækgaard Lauritsen. We also thank Cheng-Zhi Zou from NOAA for discussions and for information on the IMICA data set and the NOAA antenna correction. The AMSU-A CDR used in this study was acquired from NOAA's National Climatic Data Center (http://www.ncdc.noaa.gov).

References

Anthes, R. A., et al. (2008), The COSMIC/FORMOSAT-3 mission: Early results, *Bull. Am. Meteorol. Soc.*, *89*(3), 313–333, doi:10.1175/BAMS-89-3-313.

Buehler, S. A., M. Kuvatov, and V. O. John (2005), Scan asymmetries in AMSU-B data, *Geophys. Res. Lett.*, *32*, L24810, doi:10.1029/2005GL024747.

Buehler, S. A., N. Courcoux, and V. O. John (2006), Radiative transfer calculations for a passive microwave satellite sensor: Comparing a fast model and a line-by-line model, *J. Geophys. Res.*, *111*, D20304, doi:10.1029/2005JD006552.

Buehler, S. A., P. Eriksson, and O. Lemke (2011), Absorption lookup tables in the radiative transfer model ARTS, *J. Quant. Spectrosc. Radiat. Transfer*, *112*(10), 1559–1567, doi:10.1016/j.jqsrt.2011.03.008.

Chen, X., and X. Zou (2014), Postlaunch calibration and bias characterization of AMSU-A upper air sounding channels using GPS RO data, *J. Geophys. Res. Atmos.*, *119*, 3924–3941, doi:10.1002/2013JD021037.

Doherty, A., N. Atkinson, W. Bell, B. Candy, S. Keogh, and C. Cooper (2012), An initial assessment of data from the Advanced Technology Microwave Sounder, Forecast R&T Report no. 569, *Tech. Rep.*, U. K. MetOffice, Exeter, U. K.

Eriksson, P., M. Ekström, C. Melsheimer, and S. A. Buehler (2006), Efficient forward modelling by matrix representation of sensor responses, *Int. J. Remote Sens.*, *27*(9–10), 1793–1808, doi:10.1080/01431160500447254.

Eriksson, P., S. A. Buehler, C. P. Davis, C. Emde, and O. Lemke (2011), ARTS, the atmospheric radiative transfer simulator, version 2, *J. Quant. Spectrosc. Radiat. Transfer*, *112*(10), 1551–1558.

Feltz, M. L., R. O. Knuteson, H. E. Revercomb, and D. C. Tobin (2014), A methodology for the validation of temperature profiles from hyperspectral infrared sounders using GPS radio occultation: Experience with AIRS and COSMIC, *J. Geophys. Res. Atmos.*, *119*, 1680–1691, doi:10.1002/2013JD020853.

Foelsche, U., B. Scherllin-Pirscher, F. Ladstädter, A. K. Steiner, and G. Kirchengast (2011a), Refractivity and temperature climate records from multiple radio occultation satellites consistent within 0.05%, *Atmos. Meas. Tech.*, *4*(9), 2007–2018, doi:10.5194/amt-4-2007-2011.

Foelsche, U., S. Syndergaard, J. Fritzer, and G. Kirchengast (2011b), Errors in GNSS radio occultation data: Relevance of the measurement geometry and obliquity of profiles, *Atmos. Meas. Tech.*, *4*(2), 189–199, doi:10.5194/amt-4-189-2011.

He, W., C. Zou, and H. Chen (2014), Validation of AMSU-A measurements from two different calibrations in the lower stratosphere using COSMIC radio occultation data, *Chin. Sci. Bull.*, *59*(11), 1159–1166, doi:10.1007/s11434-014-0125-9.

Hewison, T., and R. Saunders (1996), Measurements of the AMSU-B antenna pattern, *IEEE Trans. Geosci. Remote Sens.*, *34*(2), 405–412, doi:10.1109/36.485118.

Ho, S.-P., M. Goldberg, Y.-H. Kuo, C.-Z. Zou, and W. Schreiner (2009), Calibration of temperature in the lower stratosphere from microwave measurements using COSMIC radio occultation data: Preliminary results, *Terr. Atmos. Oceanic Sci.*, *20*, 87–100.

Jin, S., E. Cardellach, and F. Xie (2014), *GNSS Remote Sensing Theory, Methods and Applications, Remote Sensing and Digital Image Processing*, chap. 6, pp. 121–157, vol. 19, Springer, Dordrecht, Netherlands.

Kursinski, E. R., G. A. Hajj, T. Schofield, R. P. Linfield, and K. R. Hardy (1997), Observing Earth's atmosphere with radio occultation measurements using the Global Positioning System, *J. Geophys. Res.*, *102*, 23,429–23,465.

Labrot, T., N. Atkinson, and P. Roquet (2014), AAPP documentation software description, version 7.4 — Document NWPSAF-MF-UD-002, Tech. rep., Satellite Application Facility for Numerical Weather Prediction (NWPSAF), available from MetOffice, Exeter, U. K.

Ladstädter, D. F. (2011), Co-locating GRAS with nadir sounders onboard Metop: An assessment for instrument and climate monitoring GRAS SAF CDOP Visiting Scientist report 7 Ref: SAF/GRAS/DMI/REP/VS07/001, Tech. Rep. VS07, Radio Occultation Meteorology Satellite Application Facility (ROMSAF), Copenhagen. [Available at http://www.romsaf.org.]

Ladstädter, D. F., A. K. Steiner, U. Foelsche, L. Haimberger, C. Tavolato, and G. Kirchengast (2011), An assessment of differences in lower stratospheric temperature records from (A)MSU, radiosondes, and GPS radio occultation, *Atmos. Meas. Tech.*, *4*(9), 1965–1977, doi:10.5194/amt-4-1965-2011.

Lu, Q., and W. Bell (2013), Characterising channel center frequencies in AMSU-A and MSU microwave sounding instruments, *Tech. Rep.*, ECMWF, Reading, U. K.

Melsheimer, C., et al. (2005), Intercomparison of general purpose clear sky atmospheric radiative transfer models for the millimeter/submillimeter spectral range, *Radio Sci.*, *40*, RS1007, doi:10.1029/2004RS003110.

Mo, T. (1999), AMSU-A antenna pattern corrections, *IEEE Trans. Geosci. Remote Sens.*, *37*(1), 103–112, doi:10.1109/36.739131.

Mo, T. (2011), Calibration of the NOAA AMSU-A radiometers with natural test sites, *IEEE Trans. Geosci. Remote Sens.*, *49*(9), 3334–3342, doi:10.1109/TGRS.2011.2104417.

NOAA (2012), POLAR spacecraft status as of: Tues 3 Jan 2012, 08:00 EST.

Qin, Z., X. Zou, and F. Weng (2012), Comparison between linear and nonlinear trends in NOAA-15 AMSU-A brightness temperatures during 1998–2010, *Clim. Dyn.*, *39*(7-8), 1763–1779, doi:10.1007/s00382-012-1296-1.

Robel, J., et al. (2009), NOAA KLM user's guide with NOAA-N, -N' supplement, Tech. rep., National Oceanic and Atmospheric Administration, National Environmental Satellite, Data, and Information Service, National Climatic Data Center, Remote Sensing and Applications Division, Asheville, N. C.

Rosenkranz, P. W. (1993), Absorption of microwaves by atmospheric gases, in *Atmospheric Remote Sensing by Microwave Radiometry*, edited by M. A. Janssen, chap. 2, pp. 37–90, John Wiley, New York.

Schrøder, T., S. Leroy, M. Stendel, and E. Kaas (2003), Validating the microwave sounding unit stratospheric record using GPS occultation, *Geophys. Res. Lett.*, *30*(14), 1734, doi:10.1029/2003GL017588.

Steiner, A., G. Kirchengast, M. Borsche, and U. Foelsche (2009), Lower stratospheric temperatures from CHAMP RO compared to MSU/AMSU records: An analysis of error sources, in *New Horizons in Occultation Research*, edited by A. Steiner et al., pp. 219–234, Springer, Berlin.

Steiner, A. K., G. Kirchengast, M. Borsche, U. Foelsche, and T. Schoengassner (2007), A multi-year comparison of lower stratospheric temperatures from CHAMP radio occultation data with MSU/AMSU records, *J. Geophys. Res.*, *112*, D22110, doi:10.1029/2006JD008283.

Verdes, C. L., S. A. Buehler, A. Perrin, J.-M. Flaud, J. Demaison, G. Wlodarczak, J.-M. Colmont, G. Cazzoli, and C. Puzzarini (2005), A sensitivity study on spectroscopic parameter accuracies for a mm/sub-mm limb sounder instrument, *J. Mol. Spectrosc.*, *229*(2), 266–275, doi:10.1016/j.jms.2004.09.014.

von Engeln, A., Y. Andres, C. Marquardt, and F. Sancho (2011), GRAS radio occultation on-board of Metop, *Adv. Space Res.*, *47*(2), 336–347, doi:10.1016/j.asr.2010.07.028.

Wang, W., and C.-Z. Zou (2014), AMSU-A-only atmospheric temperature data records from the lower troposphere to the top of the stratosphere, *J. Atmos. Oceanic Technol.*, *31*, 808–825.

Woolf, H., P. van Delst, and W. Zhang (1999), NOAA-15 HIRS/3 and AMSU transmittance model validation, *Technical Proceedings of the International ATOVS Study Conference, 10th*, Boulder, Colo.

Zou, C.-Z., and W. Wang (2011), Intersatellite calibration of AMSU-A observations for weather and climate applications, *J. Geophys. Res.*, *116*, D23113, doi:10.1029/2011JD016205.

Zou, C.-Z., and W. Wang (2013), Climate algorithm theoretical basis document (C-ATBD) — AMSU radiance fundamental climate data record derived from integrated microwave inter-calibration approach, *Tech. Rep.*, NOAA, Asheville, N. C.

Zou, C.-Z., M. D. Goldberg, Z. Cheng, N. C. Grody, J. T. Sullivan, C. Cao, and D. Tarpley (2006), Recalibration of microwave sounding unit for climate studies using simultaneous nadir overpasses, *J. Geophys. Res.*, *111*, D19114, doi:10.1029/2005JD006798.

Zou, X., L. Lin, and F. Weng (2014), Absolute calibration of ATMS upper level temperature sounding channels using GPS RO observations, *IEEE Trans. Geosci. Remote Sens.*, *52*(2), 1397–1406, doi:10.1109/TGRS.2013.2250981.